



Substituted azomethine–zinc complexes: Thermal stability, photophysical, electrochemical and electron transport properties

Liang Chen, Juan Qiao*, Junfeng Xie, Lian Duan, Deqiang Zhang, Liduo Wang, Yong Qiu

Key Lab of Organic Optoelectronics & Molecular Engineering of Ministry of Education, Department of Chemistry, Tsinghua University, Beijing 100084, China

ARTICLE INFO

Article history:

Received 6 August 2006
Received in revised form 13 October 2008
Accepted 15 October 2008
Available online 25 October 2008

Keywords:

Salicylidene–aniline
Zinc complex
Electron transport
OLEDs

ABSTRACT

A series of zinc complexes with salicylidene–aniline and its derivatives as ligands have been designed and synthesized for electron transport in organic light-emitting diodes (OLEDs). A systematic study on their thermal, photophysical, electrochemical and electron transport properties has been carried out and demonstrated that the substitution of $-\text{CH}_3$, $-\text{OCH}_3$, $-\text{CN}$ and $-\text{N}(\text{CH}_3)_2$ on aniline ring of ligands can finely tune the properties of the corresponding zinc complexes. The density functional theory calculations of location and distribution of the frontier molecular orbital states unveiled the relationships between the substituents and the photophysical and electrochemical properties of these complexes. OLEDs with bis(salicylidene-*p*-methylaniline)zinc(II) ($\text{Zn}(\text{sama})_2$) as the electron transport layer exhibited high current efficiency, indicating its great potential as a useful electron transport material for OLEDs.

© 2008 Elsevier B.V. All rights reserved.

1. Introduction

Vacuum-deposited organic light-emitting diodes (OLEDs) have made great progress since the first report by Tang and VanSlyke of strong green electroluminescence from tris(8-hydroxyquinoline)aluminum (Alq_3) [1]. Alq_3 is the most widely used emitting material and electron transport host because of its environmental stability with high glass transition temperature (T_g) and ease of sublimation to form amorphous thin film [2,3]. Up to now, many other organic metal chelates have been reported as emitting materials or electron transport hosts. By introducing other central metal atoms (Ga, In, Sc [4], Be, Mg, Zn [5]...), a variety of metal complexes with 8-hydroxyquinoline have been designed and synthesized for use in OLEDs [6].

It is well known that the electron mobility of Alq_3 is much lower than the hole mobility of conventional hole transport materials such as *N,N'*-diphenyl-*N,N'*-bis(3-methyl)-benzidine (TPD) and *N,N'*-diphenyl-*N,N'*-bis(1-naphthyl)-benzidine (NPB) [7]. The imbalance of two charge carriers reduces the quantum efficiency for light emitting [8], then new electron transport materials with higher electron mobility are highly desirable. Recently, zinc complexes have been introduced to OLEDs and recognized as useful electron transport materials, e.g. bis(8-hydroxyquinoline)zinc

(Znq_2) [5,9] and bis(2-(1-hydroxyphenyl)benzothiazolate)zinc ($\text{Zn}(\text{BTZ})_2$) [10,11] have proven to possess higher electron mobilities than Alq_3 . Azomethine–zinc complexes with Schiff-base ligands have previously been studied about their structures and reactions [12–16]. Though they were used as the emitting layer in OLEDs research by Hamada and co-workers [17] in 1993, more reports on material properties and corresponding device performance about these zinc complex derivatives are needed. In this paper, we synthesized five zinc complexes with different Schiff-base ligands, bis(salicylidene–aniline)zinc(II) ($\text{Zn}(\text{saa})_2$), bis(salicylidene-*p*-methylaniline)zinc(II) ($\text{Zn}(\text{sama})_2$), bis(salicylidene-*p*-methoxyaniline)zinc(II) ($\text{Zn}(\text{saoma})_2$), bis(salicylidene-*p*-methoxyaniline)zinc(II) ($\text{Zn}(\text{saoa})_2$), and bis[salicylidene(4-dimethylamino)aniline]zinc(II) ($\text{Zn}(\text{sada})_2$), as shown in Fig. 1a. Amongst these compounds, $\text{Zn}(\text{saa})_2$, $\text{Zn}(\text{sama})_2$, $\text{Zn}(\text{saoma})_2$ and $\text{Zn}(\text{sada})_2$ have previously been reported by different groups [13,15,18,19]. Here, a detailed investigation of the molecular structure, thermal stability as well as the photoluminescent, electrochemical and electron transport properties was carried out. It was found that the steric structure and electronegativity of substitution groups have a large effect on the electrochemical and photophysical behaviors of the corresponding complexes. With the assistance of quantum chemical calculation, we further studied the distribution of molecular orbitals and the effect of substitution on the electronic structures of these zinc compounds. Finally, the device performance demonstrated that $\text{Zn}(\text{sama})_2$ might be a useful electron transport material for OLEDs.

* Corresponding author. Tel.: +86 10 62773109; fax: +86 10 62795137.

E-mail addresses: qjuan@mail.tsinghua.edu.cn (J. Qiao), qiuy@mail.tsinghua.edu.cn (Y. Qiu).

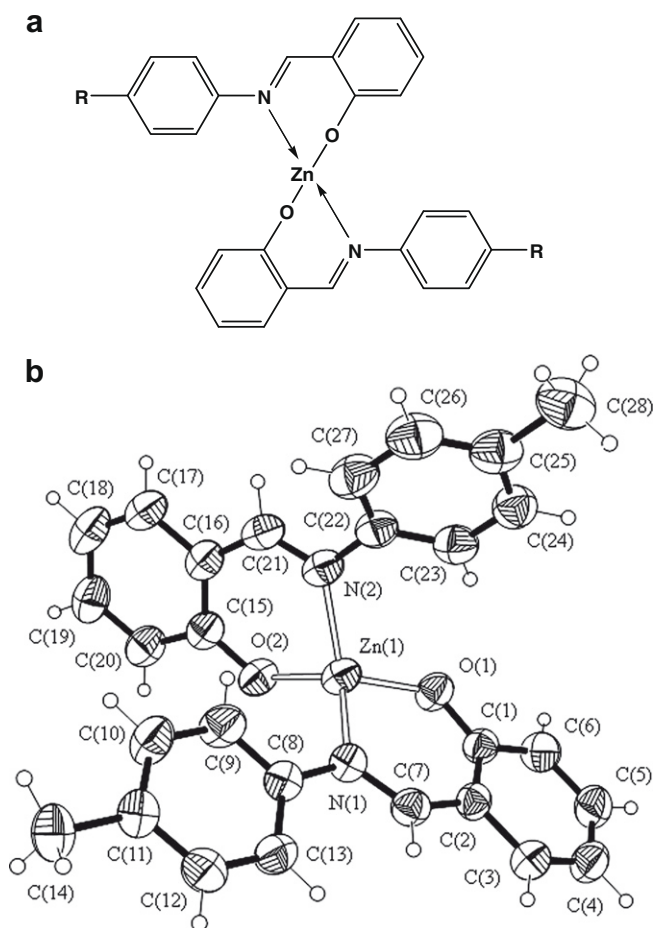


Fig. 1. (a) Molecular formulas of the zinc complexes used in this study. R = H, Zn(saa)₂; R = CH₃, Zn(sama)₂; R = OCH₃, Zn(saoa)₂; R = CN, Zn(saca)₂; R = N(CH₃)₂, Zn(sada)₂. (b) ORTEP drawing of Zn(sama)₂ with 35% probability ellipsoids.

2. Experimental

2.1. Synthesis and structure characterization

The preparation and purification of Schiff-base ligands and corresponding zinc complexes were similar to synthesis of Zn(sada)₂ described in our first paper [19] about Zn(sada)₂.

The Schiff-base ligand was synthesized by refluxing a mixture of salicylaldehyde and corresponding substituted aniline in a 1:1 molar ratio and the following recrystallization with ethanol gave a precipitate with a yield of about 90%.

The zinc complex was prepared through a reaction between ZnCl₂ and corresponding Schiff-base ligand. A solution of ZnCl₂ (0.6815 g, 5 mmol) in ethanol (30 ml) was gradually added to a mixed solution of Schiff-base ligand (5 mmol) and piperidine (1.0 ml, 10 mmol) in 120 ml ethanol. The mixture while being heated at reflux for 0.5 h, and then stirred at room temperature for 24 h. All the products are light yellow precipitates. The crude products were collected by filtration and washed with ethanol, and finally dried under an infrared lamp. The crude product yields are around 70–87%. The materials were further purified by vacuum train sublimation before analysis and the fabrications of devices.

Zn(saa)₂: MS (EI, 70 eV): [*m/z*] 457. Elemental Anal. Calc. for C₂₆H₂₀N₂O₂Zn (457.8): C, 68.21; H, 4.40; N, 6.12. Found: C, 68.01; H, 4.32; N, 6.33%. ¹H NMR (400 MHz, [*d*₆]DMSO, 25 °C, TMS), δ = 6.52 (t, 2H, *J* = 7.3 Hz), 6.62 (d, 2H, *J* = 8.5 Hz), 7.28 (m, 4H), 7.43 (m, 6H), 7.62 (d, 4H, *J* = 7.9 Hz), 8.54 (s, 2H).

Zn(sama)₂: MS (EI, 70 eV): [*m/z*] 484. Elemental Anal. Calc. for C₂₈H₂₄N₂O₂Zn (485.9): C, 69.21; H, 4.98; N, 5.77. Found: C, 69.36; H, 4.98; N, 5.99%. ¹H NMR (400 MHz, [*d*₆]DMSO, 25 °C, TMS), δ = 2.23 (s, 6H), 6.65 (m, 2H), 6.73 (d, 2H, *J* = 8.5 Hz), 7.14 (d, 4H, *J* = 8.4 Hz), 7.19 (d, 4H, *J* = 8.4 Hz), 7.35 (ddd, 2H, *J* = 8.7, 7.0, 1.8 Hz), 7.50 (dd, 2H, *J* = 8.0, 1.6 Hz), 8.78 (s, 2H).

Zn(saoa)₂: MS (EI, 70 eV): [*m/z*] 516. Elemental Anal. Calc. for C₂₈H₂₄N₂O₄Zn (517.9): C, 64.94; H, 4.67; N, 5.41. Found: C, 64.72; H, 4.64; N, 5.81%. ¹H NMR (400 MHz, [*d*₆]DMSO, 25 °C, TMS), δ = 3.70 (s, 6H), 6.65 (m, 2H), 6.91 (m, 4H), 7.27 (m, 4H), 7.34 (ddd, 2H, *J* = 8.5, 6.9, 1.6 Hz), 7.50 (dd, 2H, *J* = 7.9, 1.5 Hz), 8.77 (s, 2H).

Zn(saca)₂: MS (EI, 70 eV): [*m/z*] 506. Elemental Anal. Calc. for C₂₈H₁₈N₄O₂Zn (507.8): C, 66.22; H, 3.57; N, 11.03. Found: C, 66.02; H, 3.60; N, 11.23%. ¹H NMR (400 MHz, [*d*₆]DMSO, 25 °C, TMS), δ = 6.59 (t, 2H, *J* = 8.6 Hz), 7.33 (ddd, 2H, *J* = 8.6, 7.8, 1.7 Hz), 7.41 (dd, 2H, *J* = 7.8, 1.6 Hz), 7.54 (m, 4H), 7.84 (d, 4H, *J* = 7.7 Hz), 8.57 (s, 2H).

The single crystal structure of Zn(sama)₂ was analyzed by X-ray diffraction and the result is similar with the previous report by other group.[15] The ORTEP drawing of Zn(sama)₂ with 35% probability ellipsoids is illustrated in Fig. 1b to show the stereochemistry of this complex.

2.2. Equipment

EI-MS spectra were obtained from a TRIO-2000 mass spectrophotometer. Element analysis data were obtained from a Elementar Vario EL CHN element analysis instrument. ¹H NMR spectra were recorded on a Burkert ARX400 NMR spectrometer with tetramethylsilane as internal standard. Thermal analysis was determined by differential scanning calorimetry (DSC) and thermal gravimetric analysis (TGA) performed using TA DSC 2910 Modulated instrument and TA TGA 2050 instrument, respectively. Absorption spectra were recorded with an Agilent 8453 UV–Vis spectrophotometer, and PL spectra were obtained from a HORABA FluoroMax-3 spectrofluorimeter, respectively. PL quantum efficiencies (Φ_{PL}) were determined from dimethyl formamide (DMF) solutions by controlling the concentration of the sample so that the absorbance at 390 nm (excitation wavelength) was lower than 0.2 absorption unit. All the Φ_{PL} of samples were calculated with the known value for Alq₃ in DMF ($\Phi_{PL} = 0.116$) [20] as reference. Cyclic voltammetry measurements were conducted on a model CH 600 voltammetric analyzer with a platinum plate as the working electrode, a silver wire as the pseudo-reference electrode, a polished platinum wire as the counter electrode, and ferrocene as an internal reference [21], at a scan rate of 50 mV/s. The supporting electrolyte was 0.1 mol/L tetrabutylammonium tetrafluoroborate in DMF, the solution was deoxygenated with bubbling nitrogen for 15 min. The energy levels of highest occupied molecular orbital (HOMO) and lowest unoccupied molecular orbital (LUMO) were calculated from the oxidation and reduction potentials by adding 4.4, respectively [22].

2.3. Density functional theory calculations

The density functional theory (DFT) was employed by using GAUSSIAN 03 package [23] in this study. The restricted B3LYP (Becke three-parameter Lee–Yang–Parr, for neutral molecules) and restricted-open B3LYP (for ions) exchange–correlation functional, which combines the Becke three-parameter exchange functional [24] with the gradient-corrected correlation functional of Lee et al. [25], was used for all calculations. We chose the basis 6-31g(d) and performed the full optimizations for the geometrical structures and electron distributions of HOMO and LUMO of neutral Zn(saa)₂, Zn(sama)₂ and Zn(sada)₂. In addition, cation and an-

ion of Zn(sama)_2 (the neutral molecule in the presence of an extra hole and that of an extra electron, respectively) were also calculated. The initial geometric parameters employed in our calculations are from the crystal structure data [15,19].

2.4. Fabrication of devices

Devices were fabricated on a glass slides coated with indium tin oxide (ITO) with $30 \Omega/\text{square}$ using a conventional vacuum vapor deposition in a vacuum of around 10^{-3} Pa. ITO substrates were cleaned by ultrasonication in ethanol–acetone (1:1) and de-ionized water successively, and were then dried under infrared lamp for 2 h before use. After deposition of the organic layers, Mg and Ag were coevaporated from separate evaporation boats in a 10:1 atomic ratio (Mg:Ag) to form a 150 nm alloy layer, then followed by a 50 nm Ag cap without breaking the vacuum. The luminance–current–voltage characteristics were measured with a Keithley 4200 semiconductor characterization system. All the measurements were carried out in air without encapsulation of the devices.

3. Results and discussion

3.1. Thermal stability

Thermal events observed in DSC and TGA curves can be attributed to several phase transitions of materials in heating process. The weight loss 3% temperature can be obtained in TGA curve, and the melting point (T_m), glass transition point (T_g) and recrystallization point (T_{c1}) were measured from DSC cycle, respectively. Results are presented in Table 1.

Despite of the similarity of ligands and coordination environments, the complexes with $-\text{CN}$, $-\text{OCH}_3$, $-\text{CH}_3$ as substitutions exhibit relatively lower weight loss 3% temperatures. The trend in thermal sublimation temperatures increases in the order of $\text{Zn(saca)}_2 < \text{Zn(saoo)}_2 < \text{Zn(sama)}_2 < \text{Zn(sada)}_2 \sim \text{Zn(saa)}_2$.

The strong polar group $-\text{CN}$ or $-\text{N}(\text{CH}_3)_2$ increases the molecular dipole and the Van der Waals force inner crystal and glass state, as a result, Zn(saca)_2 and Zn(sada)_2 have much higher melting and glass transition points. Among these compounds, Zn(saa)_2 is the only one without observable glass transition. It is suggested that Zn(saa)_2 can not form stable glass state. The surface morphology study of vapor-deposited films on ITO substrates by atomic force microscope (AFM) was explored subsequently and demonstrated that the thin films of these zinc complexes except Zn(saa)_2 , exhibit an entirely amorphous, uniform surface and a negligible change after being exposed in air at room temperature for 5 days.

In contrast to Zn(sama)_2 and Zn(saca)_2 , the second heating cycles of Zn(saoo)_2 and Zn(sada)_2 do not reveal a recrystallization exotherm (T_{c1}) following glass transition. Such recrystallization of glass state is one of the most potential approaches to reduce the stability of amorphous thin films. Non-planar substitution groups ($-\text{OCH}_3$ and $-\text{N}(\text{CH}_3)_2$) may increase the vibrational and rotational degrees of freedom of the whole molecules, thereby preventing easy packing of molecules and hence ready crystallization.

Table 1
Thermal analysis data.

Zinc complexes	Weight loss 3% temperature ($^{\circ}\text{C}$)	T_m ($^{\circ}\text{C}$)	T_g ($^{\circ}\text{C}$) ^a	T_{c1} ($^{\circ}\text{C}$) ^a
Zn(saa)_2	317	186	n.	n.
Zn(sama)_2	301	208	82	144
Zn(saoo)_2	282	191	80	n.
Zn(saca)_2	279	250	119	170
Zn(sada)_2	317	274	112	n.

^a n. = not exist or not observable.

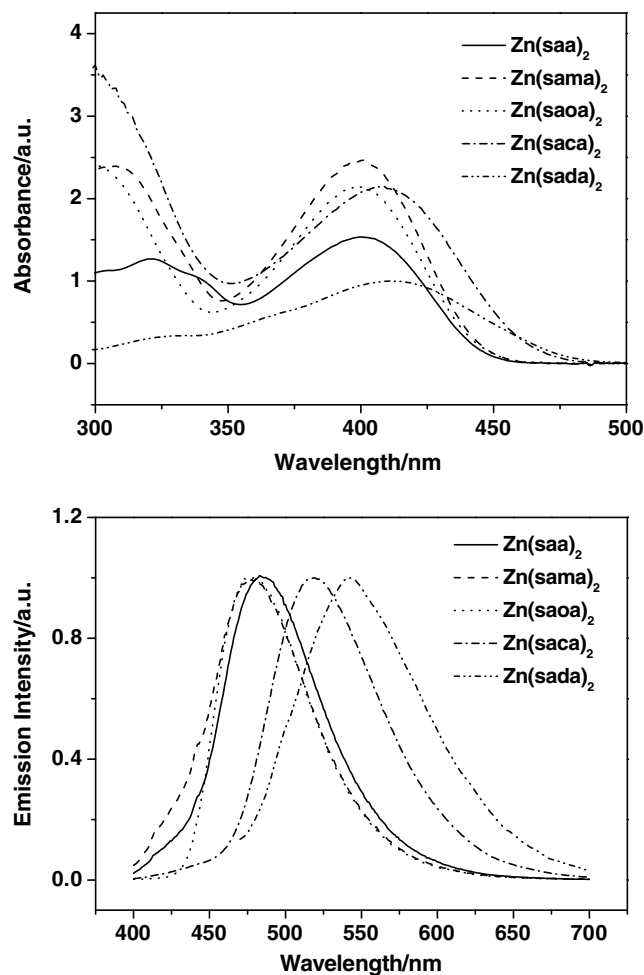


Fig. 2. Absorption and PL emission spectra of zinc complexes in DMF solutions.

Table 2
Photophysical data in DMF solution.

zinc complexes	Abs. λ_{max} (nm) ^a	Abs. shift (nm) ^b	Emission λ_{max} (nm) ^a	Emission shift (nm) ^b	Φ_{PL}
Zn(saa)_2	400	–	487	–	0.057
Zn(sama)_2	401	+1	480	–7	0.031
Zn(saoo)_2	400	0	480	–7	0.011
Zn(saca)_2	409	+9	520	+33	0.012
Zn(sada)_2	412	+12	553	+66	0.007

^a All data were obtained in DMF solution (10^{-5} mol/L).

^b Shift from Zn(saa)_2 .

Table 3
Electrochemical data in DMF solution.

Zinc complexes	HOMO (eV)	LUMO (eV)	E_g (eV)
Zn(saa)_2	–5.8	–3.1	2.7
Zn(sama)_2	–5.8	–2.9	2.9
Zn(saoo)_2	–5.6	–2.7	2.9
Zn(saca)_2	–5.8	–3.2	2.6
Zn(sada)_2	–5.1	–2.5	2.6

3.2. Photophysical properties

The electron transition responsible for photoluminescence in these zinc complexes is originated from Schiff-base ligands. The

absorption and PL spectra of the zinc complexes in DMF solutions are shown in Fig. 2, and the main photophysical data are list in Table 2. The λ_{max} of absorption and luminescence of the corre-

sponding complexes have the similar red-shift trend in the order of $\text{Zn}(\text{saoa})_2 = \text{Zn}(\text{sama})_2 < \text{Zn}(\text{saa})_2 < \text{Zn}(\text{saca})_2$, in accordance with the sequence of the electron donating ability of substitution groups

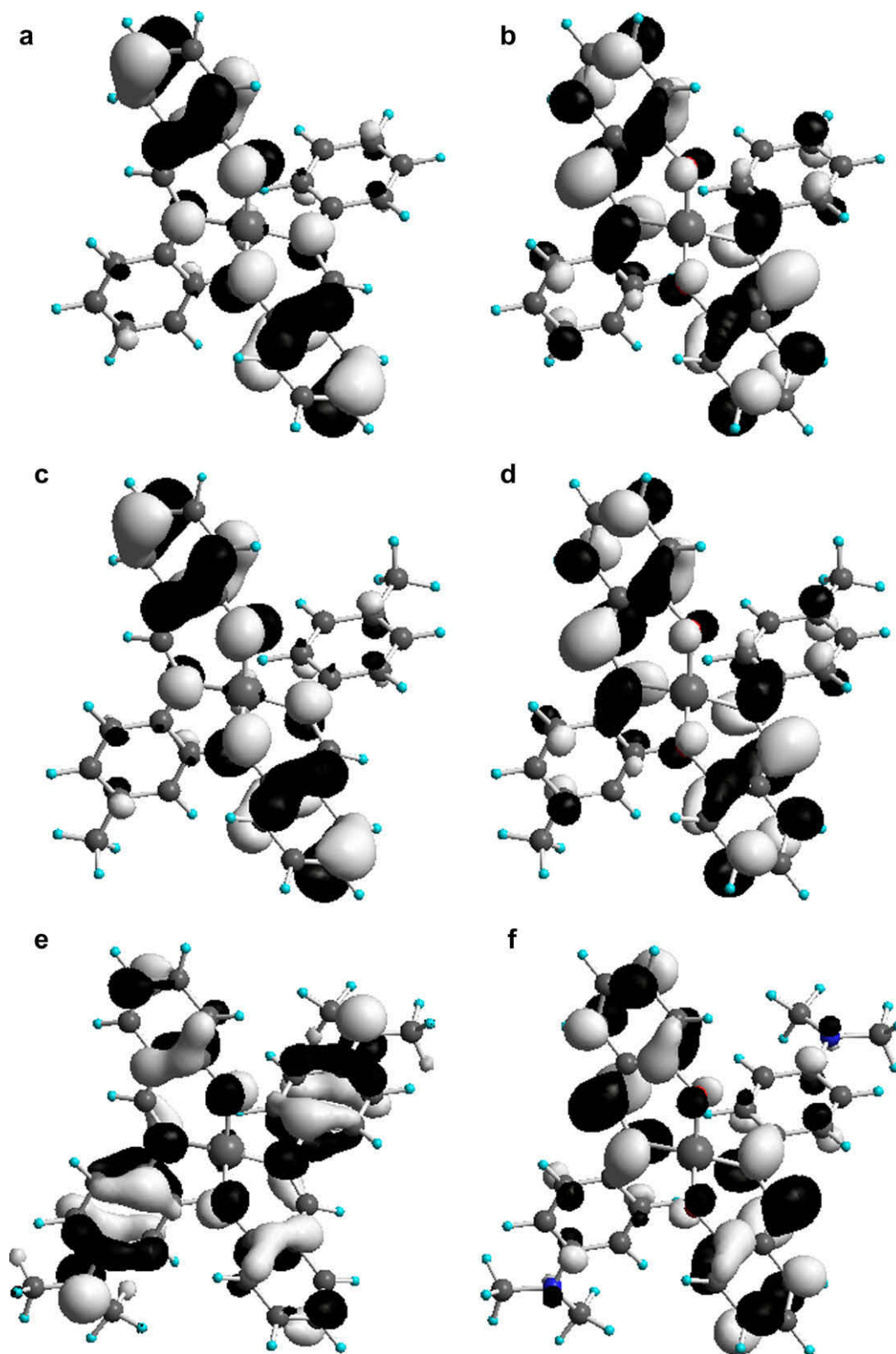


Fig. 3. Plots of the (a) HOMO of $\text{Zn}(\text{saa})_2$ molecule, (b) LUMO of $\text{Zn}(\text{saa})_2$ molecule, (c) HOMO of $\text{Zn}(\text{sama})_2$ molecule, (d) LUMO of $\text{Zn}(\text{sama})_2$ molecule, (e) HOMO of $\text{Zn}(\text{sada})_2$ molecule, and (f) LUMO of $\text{Zn}(\text{sada})_2$ molecule obtained at the RB3LYP/6-31g(d) level. All the MO surfaces correspond to an isocontour value of $|\psi| = 0.03$ a.u. Here the light grayish and darkish colors stand for the positive and negative phase of MO wavefunctions, respectively.

–OCH₃>–CH₃>–H>–CN. There is an exception that Zn(sada)₂ with the strongest electron donating group –N(CH₃)₂ exhibits the largest red-shift of PL spectrum in contrast to non-substituted Zn(saa)₂.

According to Table 2, like the reported Zn(sada)₂ [19], the ϕ_{PL} of these zinc complexes are very low, showing low potentials as the emitters in OLEDs. However, it is worth noting that non-substituted Zn(saa)₂ exhibits relative higher ϕ_{PL} . It seems that the substitutions bring a negative effect on the ϕ_{PL} , because the vibrational and rotational degrees of freedom due to the substituents increase the probability of non-radiative relaxation process.

3.3. Electrochemical properties

Energy level is an important factor for emitting and charge transport materials used in OLEDs. The injection and transport barrier of charge carriers, which is one of the key conditions that influence the operating voltage and efficiency of OLEDs, is mainly due to energetic differences between the work functions of the electrodes and HOMO or LUMO energy levels of organic materials. Experimental results are listed in Table 3.

The energy levels of HOMOs of these zinc complexes are all about 5.7 eV except Zn(sada)₂. The energy levels of LUMOs increase in the order of Zn(saca)₂<Zn(saa)₂<Zn(sama)₂<Zn(saoa)₂<Zn(sada)₂, in accord with the electronegativities of substitution groups. Among these substituent, –CN is the strongest electron withdrawing group and –N(CH₃)₂ is the strongest electron donating group. Hereby, Zn(sada)₂ possesses the highest HOMO and LUMOs. With the aid of quantum calculations, the electronic structures of the representative Zn(saa)₂, Zn(sama)₂ and Zn(sada)₂ were investigated. As seen in Fig. 3, the frontier molecular orbitals of these zinc complexes are mainly dominated by atomic orbitals originating from Schiff-base ligands in all cases and the contribution of Zn²⁺ ions is vanishingly small. For the parent complex Zn(saa)₂, both HOMO and LUMO are mainly localized on the salicylaldehyde ring of Schiff-base ligand, just a little bit of LUMO on the aniline ring. So, the substitutions of –CH₃, –OCH₃ and –CN on the aniline ring have little effect on HOMOs, but a noticeable effect on LUMOs. However, when the substitution is the strong electron donating group –N(CH₃)₂, the electron distribution of Zn(sada)₂ has largely changed, especially HOMO is delocalized on the whole ligand, not only on the salicylaldehyde ring, but also a little more on the substi-

tuted aniline ring. In addition, dimethylamino substitution group is relatively easy to be oxidized, thus resulting in an abnormal high HOMO.

To reveal the effects of charge injection on the molecular conformational stability, we have also calculated the electronic properties of both anion and cation of Zn(sama)₂. As can be seen in Fig. 4, the distribution of the extra hole in the Zn(sama)₂ cation calculated as excess spin densities is completely localized on the salicylaldehyde ring, which is similar to HOMO of neutral Zn(sama)₂, and the extra electron densities piled on the aniline ring is considerable, which is also similar to LUMO of neutral Zn(sama)₂. It is suggested that the delocalization of extra negative charge in Zn(sama)₂ is more effective, which may stabilize the anion and facilitate electron injection and transport.

The calculated adiabatic ionization potential (IP) and electron affinity (EA) of Zn(sama)₂ (IP: 6.50 eV; EA: 0.61 eV) are compared with those of Alq₃ (IP: 6.27 eV; EA: 0.52 eV). Notice that the IP and EA data of Alq₃ were reported in our previous work [26] using the same calculation method. Since the adiabatic EA value of Zn(sama)₂ is larger than that of Alq₃, i.e., Zn(sama)₂ releases more energy to create an anion than Alq₃. We may expect that Zn(sama)₂ is more likely to accept an electron and should be a more active electron transporter.

3.4. Electron transport properties

Because of its good stability of vapor-deposited amorphous thin film and potential electron injection and transport ability according to quantum calculation, Zn(sama)₂ has been used for device investigation. The “electron only” devices are used to investigate the electron transport ability of electron transport materials [27]. In our study, two “electron only” devices were fabricated with the configurations of ITO/4,7-diphenyl-1,10-phenanthroline (BPhen, 10 nm)/Zn(sama)₂ (60 nm)/Mg:Ag (device A) and ITO/BPhen (10 nm)/Alq₃ (60 nm)/Mg:Ag (device B), where BPhen was used as a hole blocking material to block hole injection from the anode. Fig. 5 shows the dependence of the current density on voltage (*I*–*V*) for devices A and B. The threshold voltages of current density (defined as the voltage required to give a current density of 1 A/m²) for devices A and B are about 3.4 V and 14.1 V, respectively, indicating that Zn(sama)₂ is more effective in electron injection than Alq₃ when the metal cathodes of OLEDs are conventional

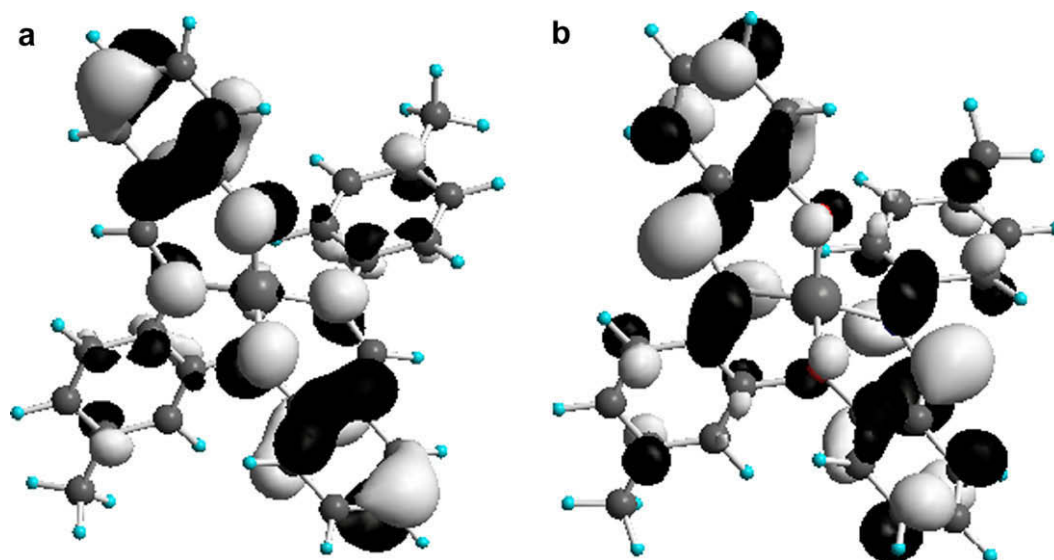


Fig. 4. Spin density surfaces of the cation (a) and anion (b) of Zn(sama)₂ obtained at the ROBLYP/6-31g(d) level. All the MO surfaces correspond to an isocontour value of $|\psi| = 0.03$ a.u. Here the light grayish and darkish colors stand for the positive and negative phase of MO wavefunctions, respectively.

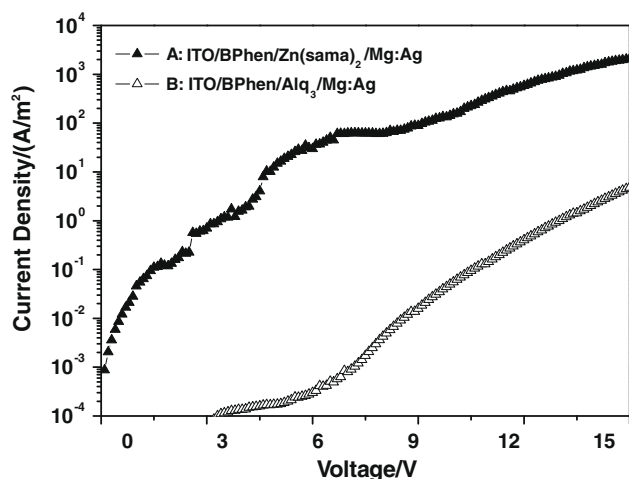


Fig. 5. Logarithmic plots of the current density–voltage characteristics of the “electron only” devices. Device A: ITO/BPhen (10 nm)/Zn(sama)₂ (60 nm)/Mg:Ag; device B: ITO/BPhen (10 nm)/Alq₃ (60 nm)/Mg:Ag.

Mg:Ag. It is well known that the electron injection barrier is determined by the difference between the work function of the metal cathode and the LUMO energy level of the used electron transport material. In this case, the work function of Mg:Ag is 3.7 eV, the energy level of LUMOs of Zn(sama)₂ and Alq₃ are 2.9 eV and 2.8 eV [28], respectively. It suggests that the OLEDs with Zn(sama)₂ as the ETL have a little lower electron injection barrier in ETL/cathode interfaces. Furthermore, at a fixed voltage, the current density of device A with Zn(sama)₂ as the ETL is significantly larger than device B with Alq₃ as the ETL. For example, at a constant voltage of 10.0 V, the current density of device A is 152 A/m², whereas device B shows only 5.55 × 10⁻² A/m². We considered that the enhancement of current density of device A is due to not only the better injection at the ETL/cathode contact, but also the intrinsic high electron mobility within Zn(sama)₂.

Two additional light emitting devices were designed and fabricated in order to further investigate the electron transport characteristics of Zn(sama)₂ in OLED: ITO / NPB (60 nm) / Alq₃ (30 nm) / Zn(sama)₂ (30 nm) / Mg:Ag (device C), and ITO / NPB (60 nm) / Alq₃ (60 nm) / Mg:Ag (device D), where NPB was used as a hole transport material. Strong green light is emitted from both devices at 520 nm, which is the characteristic luminescence from Alq₃. Fig. 6a and b contains the plots of the current density and brightness characteristics of device C and D. Device C with Zn(sama)₂ as the electron transport layer gives both higher current density and brightness at a fixed voltage, indicating that Zn(sama)₂ with matched energy level and high electron mobility enhances the injection and transport of electrons and improves the electron-hole balance. Although Zn(sama)₂ shows better electron injection and transport property than Alq₃, the current luminescent efficiency of device C (maximum: 2.60 cd/A) is lower than that of device D. Actually, the E_g of Zn(sama)₂ is 2.9 eV, which is comparable with Alq₃ with an E_g of 2.8 eV [28], therefore Zn(sama)₂ could not block the excitons generated in the emissive layer completely. The excitons injected into Zn(sama)₂ layer may quench in non-radiative relaxation process, resulting in non-effective recombination and low current efficiency.

In order to prevent the injection of holes and excitons from EML to ETL, a blocking layer aluminum (III) bis(2-methyl-8-quinolino) 4-phenylphenolate (B-Alq) was introduced into our study. The device configuration is ITO/NPB (60 nm)/Alq₃ (30 nm)/B-Alq (5 nm)/Zn(sama)₂ (25 nm)/Mg:Ag (device E). Current efficiency versus current density comparison between devices E and C are plotted in Fig. 6c. Contrast with device C, at the current density of 1340 A/

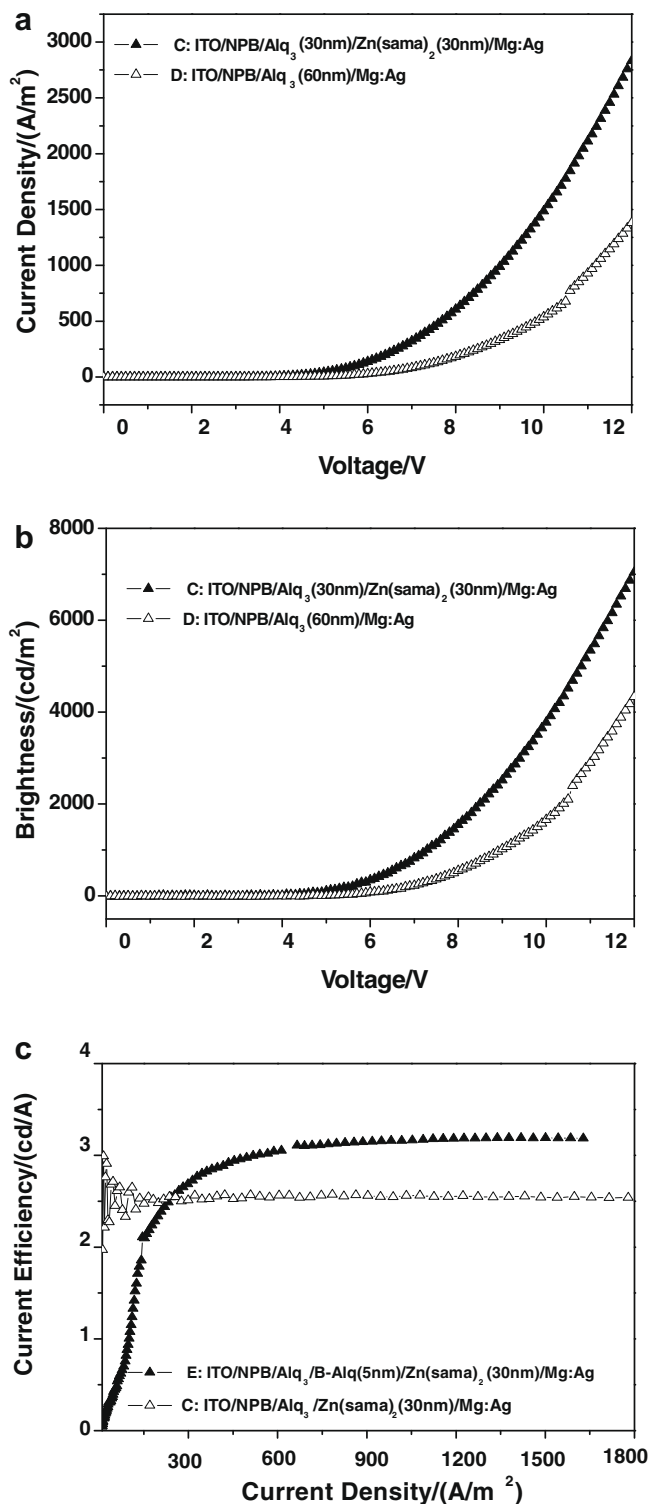


Fig. 6. (a) The current density versus voltage characteristics of devices C and D; (b) the brightness versus current voltage characteristics of devices C and D; (c) the current efficiency versus current density characteristics of devices E and C. Device C: ITO/NPB (60 nm)/Alq₃ (30 nm)/Zn(sama)₂ (30 nm)/Mg:Ag; device D: ITO/NPB (60 nm)/Alq₃ (60 nm)/Mg:Ag; device E: ITO/NPB (60 nm)/Alq₃ (30 nm)/B-Alq (5 nm)/Zn(sama)₂ (25 nm)/Mg:Ag.

m², the current efficiency of device E gives a maximum value of 3.19 cd/A. It is noted that there is no strong efficiency roll-off at high current density for device E. That means the introduction of blocking layer plays an important role in the device performance.

4. Summary

A systematic study of (salicylidene–aniline)zinc(II) complex and its derivatives on the thermal, photophysical and electrochemical and electron transport properties has been performed. These complexes are monomers of tetracoordinated zinc with distorted tetrahedron geometry. Our research demonstrated that the molar weight, conformation and electronegativity of the different substitution groups on the Schiff-base ligand can finely tune the thermal, photophysical and electrochemical properties of the corresponding Zn complexes. The sequence of the electron donating ability of substitution groups $-\text{N}(\text{CH}_3)_2 > -\text{OCH}_3 > -\text{CH}_3 > -\text{H} > -\text{CN}$ is in accordance with the height of the LUMO levels of corresponding complexes. Analysis of the electronic structure of these complexes calculated by B3LYP/6-31(d) method reveals the distribution of frontier molecular orbitals in these zinc compounds and a localization shift of HOMO in $\text{Zn}(\text{sada})_2$.

The studies of the “electron only” devices and OLEDs using $\text{Zn}(\text{sama})_2$ as the electron transport layer have confirmed the electron transport ability of $\text{Zn}(\text{sama})_2$ which is predicted by quantum calculation. Compared with typical material Alq_3 , the devices with $\text{Zn}(\text{sama})_2$ as the ETL show a better performance.

Acknowledgements

This work is supported by the National Nature Science Foundation of China (Nos. 50403001 and 50325310). We thank Center for Advanced Study, Tsinghua University for their help.

References

- [1] C.W. Tang, S.A. Van Slyke, *Appl. Phys. Lett.* 51 (1987) 913.
- [2] M. Brinkmann, G. Gadret, M. Muccini, C. Taliani, N. Masciocchi, A. Sironi, *J. Am. Chem. Soc.* 122 (2000) 5147.
- [3] L.S. Hung, C.H. Chen, *Mater. Sci. Eng. R* 39 (2002) 143.
- [4] P.E. Burrows, L.S. Sapochak, D.M. McCarty, S.R. Forrest, M.E. Thompson, *Appl. Phys. Lett.* 64 (1994) 2718.
- [5] Y. Hamada, T. Sano, M. Fujii, T. Fujii, Y. Nishio, K. Shibata, *Jpn. J. Appl. Phys.* 32 (1993) L514.
- [6] C.H. Chen, J.M. Shi, *Coord. Chem. Rev.* 171 (1998) 161.
- [7] W. Brütting, S. Berleb, A.G. Mückl, *Org. Electron.* 2 (2001) 1.
- [8] Y. Qiu, Y. Gao, P. Wei, L.D. Wang, *Appl. Phys. Lett.* 80 (2002) 2628.
- [9] L. Sapochak, F. Benincasa, R. Schofield, J. Baker, K. Riccio, D. Fogarty, H. Kohlmann, K. Ferris, P. Burrows, *J. Am. Chem. Soc.* 124 (2002) 6119.
- [10] Y. Hamada, T. Sano, M. Fujii, Y. Nishio, H. Takanashi, K. Shibata, *Jpn. J. Appl. Phys. Part 2* 35 (1996) L1339.
- [11] G. Yu, S.W. Yin, Y.Q. Liu, Z.G. Shuai, D.B. Zhu, *J. Am. Chem. Soc.* 125 (2003) 14816.
- [12] M. Dreher, H. Elias, *Z. Naturforsch.* 42b (1987) 707.
- [13] T. Sogo, J. Romero, A. Sousa, A. de Blas, M.L. Duran, *Z. Naturforsch.* 43b (1988) 611.
- [14] F.A. Bottino, P. Finocchiaro, E. Libertini, G. Mattern, *Z. Kristallogr.* 187 (1989) 71.
- [15] X.L. Liu, H.L. Chen, F.M. Miao, *Youji Huaxue* 12 (1992) 522.
- [16] F.A. Bottino, P. Finocchiaro, *Polyhedron* 4 (1985) 1507.
- [17] Y. Hamada, T. Sano, M. Fujii, Y. Nishio, K. Shibata, *Jpn. J. Appl. Phys.* 32 (1993) L511.
- [18] K.P. Dubey, C.N. Cachru, B.L. Wazir, *J. Chin. Chem. Soc.-Taip.* 26 (1979) 37.
- [19] J.F. Xie, J. Qiao, L.D. Wang, J. Xie, Y. Qiu, *Inorg. Chim. Acta* 38 (2005) 4451.
- [20] F.E. Lytle, D.R. Story, M.E. Juricich, *Spectrochim. Acta Part A* 29A (1973) 1357.
- [21] R.R. Gange, C.A. Koval, G.C. Lisensky, *Inorg. Chem.* 19 (1980) 2854.
- [22] S. Janietz, D.D.C. Bradley, M. Grell, C. Giebeler, M. Inbasekaran, E.P. Woo, *Appl. Phys. Lett.* 73 (1998) 2453.
- [23] M.J. Frisch, L.W. Trucks, H.B. Schlegel, et al., *GAUSSIAN 03*, Gaussian Inc., Pittsburgh, PA, 2003.
- [24] A.D. Becke, *Phys. Rev. A* 38 (1988) 3098.
- [25] C. Lee, W. Yang, R.G. Parr, *Phys. Rev. B* 37 (1988) 785.
- [26] J. Qiao, H. Tan, Y. Qiu, K. Balasubramanian, *J. Chem. Phys.* 124 (2006) 024719.
- [27] N. Donze, P. Pechy, M. Grätzel, M. Schaer, L. Zuppiroli, *Chem. Phys. Lett.* 305 (1999) 405.
- [28] M.T. Lee, H.H. Chen, C.H. Liao, C.H. Tsai, C.H. Chen, *Appl. Phys. Lett.* 85 (2004) 3301.